Vailable online at www.sciencedirect.com

SciVerse ScienceDirect

Energy Procedia 27 (2012) 103 – 108

Energy Procedia

SiliconPV 2012, 03-05 April 2012, Leuven, Belgium

Analysis of mono-cast silicon wafers and solar cells on industrial scale

T. Kaden[a*], K. Petter[a], R. Bakowskie[a], Y. Ludwig[a], R. Lantzsch[a], D. Raschke[a], S. Rupp[a], T. Spiess[a]

[a]*Q-Cells SE, Sonnenallee 17-21, D-06766 Bitterfeld-Wolfen, Germany*

Abstract

Mono-cast silicon recently became available in volumes relevant for industrial scale production of solar cells. At the present time, mono-cast wafers are classified by an optical determination of the <100>-grain area on the wafer. This paper discusses solar cell efficiency distributions of mono-cast wafers which we obtained in first tests using an industrial cell process. A screening process based on the optical classification turns out to be insufficient in order to obtain a narrow efficiency distribution. We used photoluminescence imaging as an additional fast inspection tool for wafers and solar cells. Prominent defects of mono-cast wafers were investigated using photoluminescence, electroluminescence and reverse biased electroluminescence (ReBEL) imaging as well as the structural defect density (SDD) method on a laboratory scale.

© 2012 Published by Elsevier Ltd. Selection and peer-review under responsibility of the scientific committee of the SiliconPV 2012 conference. Open access under CC BY-NC-ND license.

Keywords: Mono-cast silicon; Defects; Photoluminescence; Electroluminescence, ReBEL

1. Introduction

Mono-cast silicon is produced using a conventional directional solidification process with additional seed crystals placed on the bottom of the crucible and an adapted thermal profile for melting of the feedstock material and crystallisation of the ingot. In the centre part of the ingot, the material grows monocrystalline with a <100> orientation. Edge and corner areas of the ingot grow partially multicrystalline due to nucleation at the crucible. This detrimental effect is enhanced towards the top of

* Corresponding author. Tel.: +49 (3494) 6699 - 51216; fax: +49 (3494) 6699 - 54001
E-mail address: t.kaden@q-cells.com

1876-6102 © 2012 Published by Elsevier Ltd. Selection and peer-review under responsibility of the scientific committee of the SiliconPV 2012 conference. Open access under CC BY-NC-ND license.
doi:10.1016/j.egypro.2012.07.036

the ingot. The high mono-crystalline fraction and the reduced crystal defect density of mono-cast wafers offer the potential of higher solar cell efficiencies.

The development of mono-cast silicon can be considered as another example of a so-called hype cycle describing an emerging technology [1]. This hype cycle is characterized by five phases. *Phase 1* – the "technology trigger" was the development of BP Solar's Mono²-Wafer, details of which were published in 2008 [2, 3]. This was followed by an enthusiasm leading to *phase 2*, the "peak of inflated expectations" which was reached in the middle of 2011. Several companies launched mono-cast based products yielding high efficiencies and improved performances. *Phase 3*, the "trough of disillusionment" was reached rapidly at the beginning of 2012, caused by the understanding that numerous defects are present in the mono-cast material, impacting on the solar cell efficiencies. It is the intention of this paper to analyse the relation of these two properties. .

Phase 4, the "slope of enlightenment" is expected to develop a deeper understanding of the realistic potential and obstacles of the technology, followed eventually by *phase 5*, the "plateau of productivity", where the true usefulness of the new technology is demonstrated. Over which time scale and to what extent phase 4 and 5 will be realised, is currently an exciting question.

2. Mono-cast wafer classification and solar cell efficiencies

2.1. Wafer classification

Mono-cast wafers are classified by their area fraction of the <100> oriented grain applying an optical inspection system on as-cut wafers. The classification scheme differs between the different wafer suppliers but usually three classes are provided. Examples of wafers according to such classification schemes are shown in Fig. 1.

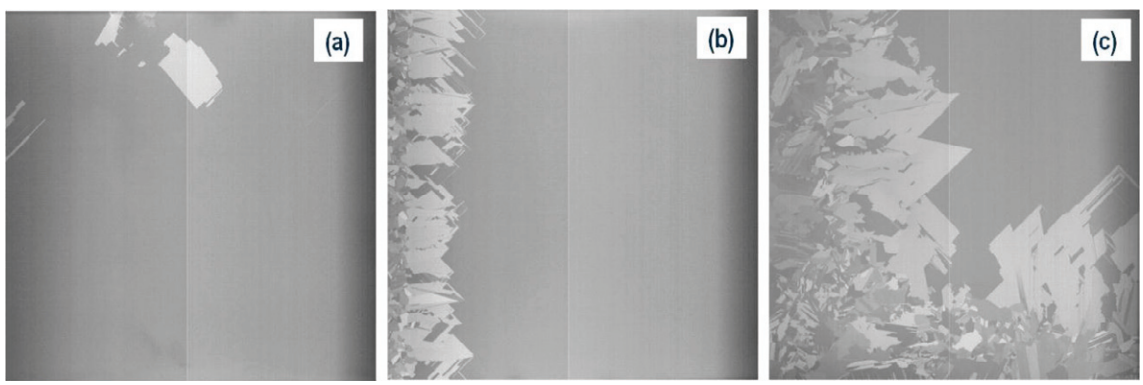

Fig. 1. Optical images of as-cut wafers taken from different mono-cast classes, clearly showing the different area fractions of the <100> oriented grain. The vertical line in the centre is due to a measurement artefact; (a) class 1; (b) class 2; (c) class 3

2.2. Solar cell efficiency distribution

In order to test the relationship between the optical classification and the solar cell efficiencies, mono-cast wafers from all three classes were tested on industrial relevant volumes using a standard back-surface field (BSF) cell process. Fig. 2 shows the comparison of the solar cell efficiency distributions of standard multicrystalline (mc-Si) and mono-cast materials of different qualities. For class 1, we found a relative increase of the distribution maximum of about 5%; see Fig. 2(a). However, the cell efficiencies are not Gauss-distributed as in the case of standard mc-Si since there is a significant broadening of the

distribution to lower cell efficiencies. Whereby class 2 still yields an increase of the distribution maximum of about 2%, class 3 can be regarded as equivalent to standard mc-Si.

It is obvious that averaging over all three distributions yields a broader efficiency distribution compared to standard mc-Si with a slight shift to higher cell efficiencies. The magnitude of this shift is determined by the relative share of these three classes over the whole ingot.

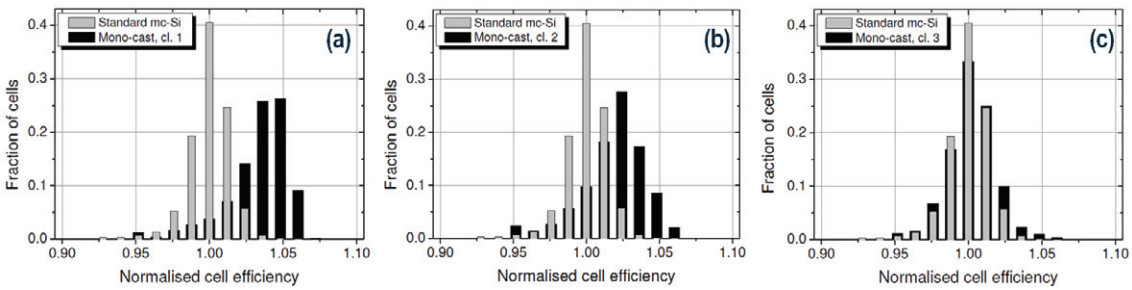

Fig. 2. Normalised solar cell efficiency distribution of different mono-cast classes in comparison to standard multicrystalline material, (a) class 1; (b) class 2; (c) class 3

2.3. Comparison of iso- and alkaline textured cells

The potential of mono-cast silicon was further evaluated by a comparison of iso- and alkaline textured solar cells. As an example for this comparison a particular brick is shown in Fig. 3. Wafers of this brick are 100% <100>-oriented from the bottom up to approximately 40% of the ingot height. The <100> orientation was once determined with electron backscatter diffraction (EBSD). In the direction of crystallisation, the monocrystalline area fraction decreases to 20% wafer area at the top of the ingot; see Fig. 3(a). Furthermore, the structural defect density (SDD), expressed in terms of the red area fraction, was measured as demonstrated by Bakowskie et al. [4]. No structural defects occur in the first 50% of the crystallisation height, above 50% the SDD increases up to a red area fraction of 8% of the wafer.

Neighbouring wafers of this brick were processed to solar cells using iso- and alkaline texture, respectively. Cell results are depicted in Fig 3(b).

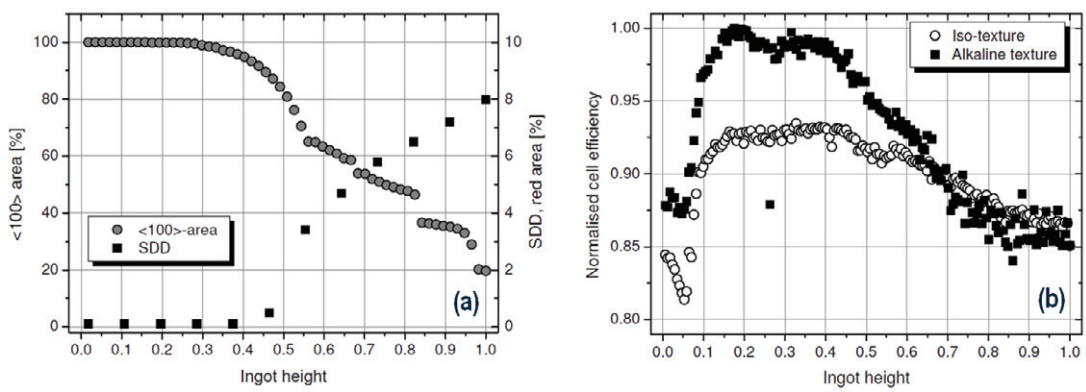

Fig. 3. (a) <100> area fraction and structural defect density (SDD) in terms of red area fraction [4] as a function of ingot height, the abrupt steps in the curve are a measurement artefact of the optical inspection; (b) solar cell efficiencies obtained with iso-texture and alkaline texture, respectively

Though being 100% monocrystalline, the bottom part yields low efficiencies for both processes due to impurity diffusion from the crucible. Between 15% and 40% of the ingot height, the alkaline textured cells show an efficiency gain up to 7.5% compared to the iso-textured cells. It should be mentioned, that the best cells reach the efficiency of Cz-Si solar cells produced with the same process. With an increasing multicrystalline fraction, the advantage of the alkaline texture decreases and vanishes completely if the area of the <100> oriented grain is below 60% of the wafer area. This is mainly due to the poor texture on the multicrystalline wafer areas.

2.4. Centre-, edge- and corner-bricks

In order to get a better understanding of the role of the <100> area fraction on the solar cell efficiency, sorted bricks from the centre, edge and corner of several mono-cast ingots were investigated. One example is shown in Fig. 4. The area fraction of the <100>-grain, represented by the grey dots, differs considerably between the three bricks as well as over the ingot height. In the centre brick, the <100>-area fraction is between 95 and 100% while in the edge brick it decreases from about 95% to 20% and in the corner from about 75% to 0%, i.e. the seeded <100>-grain orientation completely disappears.

The solar cell efficiencies, normalised to the average efficiency of our BSF process on standard mc-Si, are represented by the blue dots in Fig 4. For all bricks, the efficiency is reduced in the first 10% of the ingot height due to impurity diffusion from the crucible. These low performing parts of the ingot are normaly discarded and are only included here for scientific purposes. For the centre brick, the efficiency is 4% higher compared to the standard material up until 80% of the ingot height. It then decreases slightly. In the edge brick, the efficiency is nearly stable up to 60% ingot height and then reduces drastically. In the corner brick, the effciency continuously decreases over the ingot height. Considering the relation of <100>-area and efficiency it becomes clear, that the area of the <100>-grain is not the only parameter determining the achievable efficiency.

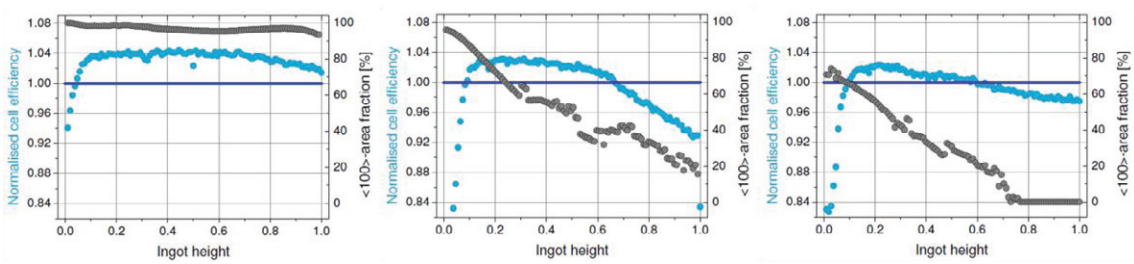

Fig. 4. Area fraction of <100>-grain orientation and solar cell efficiency bricks: (a) centre brick; (b) edge brick; (c) corner brick. The blue line designates the average efficiency of standard mc-Si solar cells

3. Defect analysis

3.1. Photoluminescence analysis of solar cells made of class 1 mono-cast wafers

The solar cell efficiency as a function of the mean photoluminescence (PL) intensity solar cells was analysed for the three mono-cast classes. As shown in Fig. 5 for solar cells made of class 1 mono-cast wafers, there is a good correlation of the solar cell efficiency and the PL intensity. This is in agreement with previous findings on mc-Si, which show a correlation of the area of dislocations as determined by PL and the cell performance, e.g. in [5].

Though having a high area fraction of the <100>-oriented grain, the efficiency of solar cells made of class 1 mono-cast wafers varies up to 8% rel. In the following, the recombination active defects which have a major influence on the cell efficiency are examined.

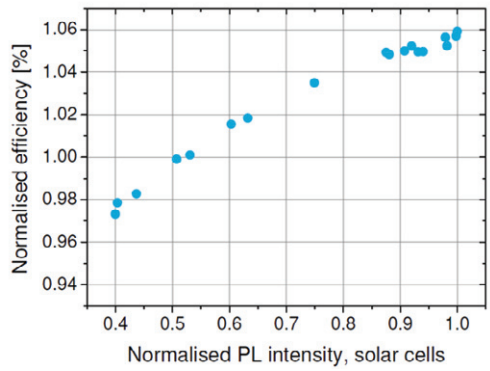

Fig. 5. Correlation of the normalised solar cell efficiency with photoluminescence (PL) intensity of solar cells

3.2. Defects originating from contact planes between seed crystals

Due to the use of a pattern of seed crystals on the bottom of the crucible, the matching of the seeds is important in order to get a high wafer quality throughout the whole ingot height. As shown in Fig. 6, there are contact planes between perfectly aligned seed crystals (upper vertical and right horizontal line) and contact planes, that have the potential to cause distorted crystal growth (lower vertical and left horizontal line). When the seeds are not perfectly matched together or the crystals are misorientated with respect to each other, these contact planes act as a source of small angle grain boundaries. Once generated, they multiply in the direction of crystallisation, as shown in Fig 6. With an increasing density of these small angle grain boundaries, the advantage of mono-cast wafers reduces significantly. However, with an exact alignment of the seed crystals the contact planes are no drawback for mono-cast silicon.

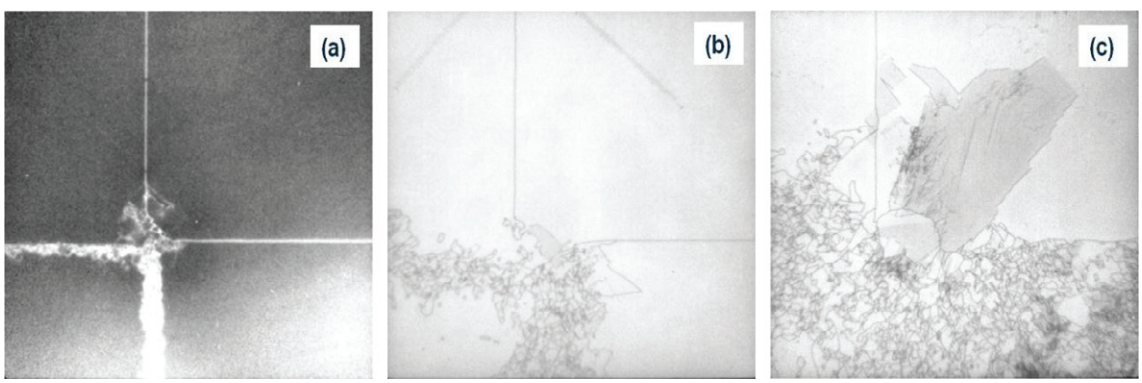

Fig. 6. Development of defects originating from seed contact planes investigated by PL; ingot height: (a) 5%; (b) 50%; (c) 95%

3.3. Classification of defects

As we have seen from the PL investigations, solar cells from wafers with a high density of small angle grain boundaries result in lower cell efficiencies. We have characterized these defects according to the recently proposed defect classification scheme by Lausch et al. [6] combining EL, sub-band EL and reverse-biased electroluminescence (ReBEL). The example in Fig. 7 reveals two recombination active defect types in the EL band-band image (Fig 7a): small angle grain boundaries all over the wafer as well as dislocations clustering in the top part. Both defects show sub-band EL (see Fig. 7b) which is significantly more intense for the small angle grain boundaries. The ReBEL image at -14V exhibits only a

pre-breakdown of the dislocation clusters (see Fig 7c). According to the classification in [6], small angle grain boundaries in mono-cast Si are a “Type B” defect, characterised by a low carrier diffusion length, no significant additional activation by high temperature steps, a high defect luminescence and a pre-breakdown behaviour of “Type III” (avalanche breakdown). The observed dislocation clusters can be classified as “Type A” defect with a lower defect luminescence and a soft pre-breakdown “Type II”.

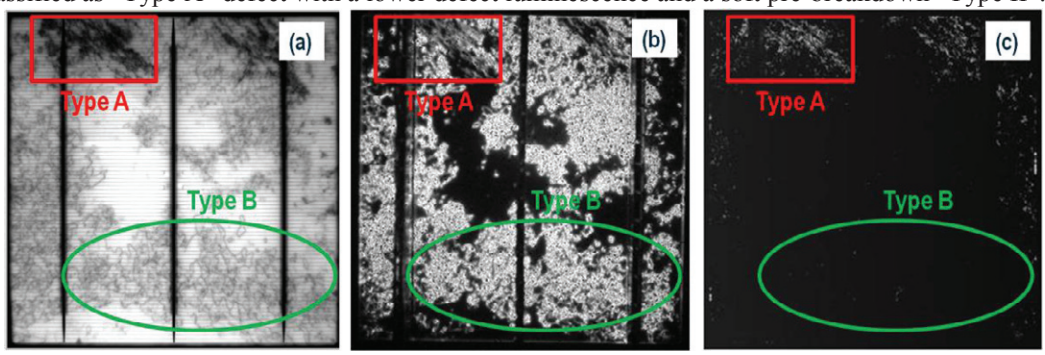

Fig. 7. (a) EL band-band image; (b) EL sub-band image; (c) ReBEL image (-14V)

4. Conclusions

We presented solar cell efficiency distributions of mono-cast silicon wafers classified by an optical determination of the <100>-grain size. A relative efficiency gain of 5% was obtained for class 1, whereas class 3 is equivalent to standard mc-Si. However, the combined distribution of these three classes, representing all wafers from throughout the entire ingot, is broadened in comparison to standard mc-Si. It was demonstrated that the optical classification scheme is not sufficient to predict a narrow solar cell efficiency distribution, which is comparable to standard mc-Si. The full potential of mono-cast silicon wafers with 100% <100>-area fraction is demonstrated with our alkaline cell process, yielding efficiencies comparable to Cz-Si. A defect analysis reveals the nature of the very prominent small angle grain boundaries, which develop under certain conditions at the interface of adjacent seed crystals and multiply in the direction of crystallisation.

Acknowledgements

This work was partly supported by the German Federal Ministry of Education and Research within the frame of the “Spitzencluster Solarvalley”, project “xμ-Material” (03SF0398E). The EL-sub and ReBEL measurements were carried out at Fraunhofer CSP Halle, which we gratefully acknowledge.

References

[1] Fenn J, Raskino M. Mastering the hype cycle. Boston: Harvard Business Press; 2008.

[2] Stoddard N, Wu B, Witting I, Wagener M, Park Y, Rozgonyi G, Clark R, Sol. State Phenomena 131-133, 1-8 (2008).

[3] Witting I, Stoddard N, Rozgonyi G, 18th Workshop on Crystalline Silicon Solar Cells & Modules: Materials and Processes, pp. 155 – 158; 2008.

[4] Bakowskie R, Kesser G, Richter R, Lausch D, Eidner A, Clemens P, Petter K, Energy Procedia, *submitted*

[5] Trupke T, Nyhus J, Haunschild J, Phys. Status Solidi RRL 5 (4), 131 – 137 (2011).

[6] Lausch D, Bakowskie R, Lorenz M, Schweizer S, Petter K, Hagendorf C, Sol. State Phenomena 178-179, 88-93 (2011).